Sensors and Materials, Vol. 35, No. 4 (2023) 1397–1411
MYU Tokyo

S & M 3255

Extension of Linear Operating Range for Linear Variable Differential Transformer Using Its Inverse Transfer Characteristic

Wandee Petchmaneelumka, Kanoknuch Songsuwankit, Apinai Rerkratn,* Rutchanee Gullayanon, and Vanchai Riewruja**

School of Engineering, King Mongkut's Institute of Technology Ladkrabang, Bangkok 10520, Thailand

(Received September 29, 2022; accepted January 18, 2023)

Keywords: linear variable differential transformer, inverse transfer characteristic, linear operating range extension, operational transconductance amplifier, hyperbolic tangent function

An analog circuit technique to realize an inverse transfer characteristic of a linear variable differential transformer (LVDT) is presented in this paper. Practically, the structure of the LVDT causes a narrow linear operating range compared with its full stroke range. However, a large linear operating range requires a huge structure for the LVDT, making it unsuitable for a small or compact measurement system. The proposed technique can be used in a commercial LVDT to extend the linear operating range to its full stroke range. The technique utilizes an inherent behavior of an operational transconductance amplifier (OTA) to emulate the LVDT transfer characteristic. The LVDT transfer characteristic generated by the OTA is used as a feedback path of the inverting amplifier formed by an operational amplifier (opamp) to realize the inverse transfer characteristic. The residual error due to the OTA behavior is very small and can be neglected without adversely affecting the performance of the proposed technique. All devices used in the proposed scheme are commercially available. The attractive features of the proposed technique are its simple configuration, small size, low cost, and high accuracy. The performance of the proposed technique is discussed in detail and confirmed by its experimental implementation. Measurement results demonstrate that the linear operating range of the commercial LVDT used in this study can be extended by a factor of more than 2.4, and a full-scale percentage error of about 0.068% was obtained.

1. Introduction

In a position measurement system, the linear variable differential transformer (LVDT) is an important inductive transducer, exhibiting excellent performance in terms of resolution, robustness, and durability.[1–5] The applications of the LVDT include the measurement of the position, force, flow, displacement, and pressure in industrial process control, building construction, automobiles, military equipment, scientific and medical equipment, and robotics.[5–15] The LVDT has a transformer-like structure, comprising a primary winding and two secondary windings connected in opposite directions. The core of the LVDT is a

*Corresponding author: e-mail: apinai.ri@kmitl.ac.th
**Corresponding author: e-mail: vanchai.ri@kmitl.ac.th
https://doi.org/10.18494/SAM4153

ISSN 0914-4935

ferromagnetic element that can be moved in the axial direction. If an excitation signal in the form of a carrier signal is applied to the primary winding, then the resulting signal from the secondary windings is in the form of amplitude modulation with suppressed carrier (AMSC).[16] This resulting signal or the difference signal from the secondary windings is usually called the LVDT signal. To obtain the displacement signal from the LVDT signal, a synchronous demodulator is required to remove the excitation signal. Several synchronous demodulators for obtaining the displacement signal from the AMSC have been proposed.[1,3,17–19] Simple synchronous demodulators using an analog multiplier and a low-pass filter or using an analog switch and an integrator have been introduced to obtain the displacement signal of the LVDT signal.[1,3,17–19] The disadvantage of these simple demodulators is that the phase shift and large time response reduce the accuracy of the displacement signal. Techniques that use a peak-amplitude finder to overcome the disadvantage of simple synchronous demodulators have recently been proposed.[16,20–21] These techniques have a fast response, high accuracy, and low cost. Unfortunately, the transfer characteristic of the displacement signal provides a narrow linear operating range for the LVDT core moved in the full-stroke range. The linear operating range of a commercial LVDT is about 10 to 30% of the size of its structure.[22,23] Therefore, a large linear operating range requires an LVDT with a huge structure, making it uneconomical and unsuitable for a compact or small-scale measurement system.

The LVDT transfer characteristic exhibits nonlinear behavior, which can be expressed as an odd function in the form of a cubic polynomial.[2,24–27] Therefore, the operating range of the LVDT is linear only in a narrow range close to the zero crossing of the LVDT transfer characteristic curve. Practically, the linear range of the LVDT is directly proportional to the size of its structure.[3] To increase the linear operating range of the LVDT by 1 mm requires an increase in the physical length of the LVDT structure by more than 50%. Modern measurement systems require compact measurement devices to simplify the configuration and reduce the total weight of the system. Therefore, the development of a small LVDT with a large linear operating range has attracted much attention. There are many approaches to enhancing the linear operating range.[22–29] A fractional-order LVDT for enhancing the linear operating range has been proposed.[22] This approach requires a special design for the LVDT structure, resulting in a high-cost device that is inconvenient to customize for a compact measurement system and has therefore not been commercialized. Techniques based on an artificial neural network have recently been introduced.[28,29] These techniques increase the linear operating range using an adaptive inverse model to compensate for the nonlinear transfer characteristic of the LVDT. The disadvantage of these techniques is that a high-speed processor is required to determine the adaptive inverse model, increasing the complexity of the configuration of the measurement system and the response time. The contrast between the size of the LVDT structure and the linear operating range can be overcome by using a circuit technique to increase the linear operating range. Approaches based on the use of an analog multiplier to generate a binomial series of the LVDT inverse transfer characteristic have also been proposed.[24–27] These approaches enable the realization of LVDTs with high accuracy, large linear operating range, and small size. However, they require high-precision analog multipliers to obtain the inverse transfer characteristic of the LVDT, resulting in a high production cost.

In this study, the linear operating range of an LVDT is increased using the LVDT inverse transfer characteristic. We propose a novel technique to extend the linear operating range of an LVDT without changing its structure, making the technique highly effective for use in a small and compact measurement system. The closed-loop principle of an operational amplifier (opamp) is used to obtain the LVDT inverse transfer characteristic. The large-signal behavior of an operational transconductance amplifier (OTA) is utilized to synthesize the odd function in the form of a cubic polynomial for the LVDT. The linear operating range of the commercial LVDT used in this study can be extended to more than 2.4 times its original value. The maximum extension of the linear range for the proposed technique is limited by the physical length of a hollow rod in the LVDT structure, where the LVDT core is only moved within the hollow rod of the LVDT structure. The performance of the proposed technique is analyzed and discussed in detail. Experimental and simulation results demonstrating the performance of the proposed circuit are included. The maximum percentage error for the core within the maximum stroke range of the LVDT used in this study was about 0.068%.

2. Principle of LVDT

The structure of the commercial LVDT is shown in Fig. 1(a). A primary winding is placed between two identical secondary windings with a hollow rod of radius r_l. The two identical secondary windings are connected in opposite directions to generate the LVDT signal. Figure 1(b) depicts a schematic diagram of the LVDT. The lengths of the primary winding and

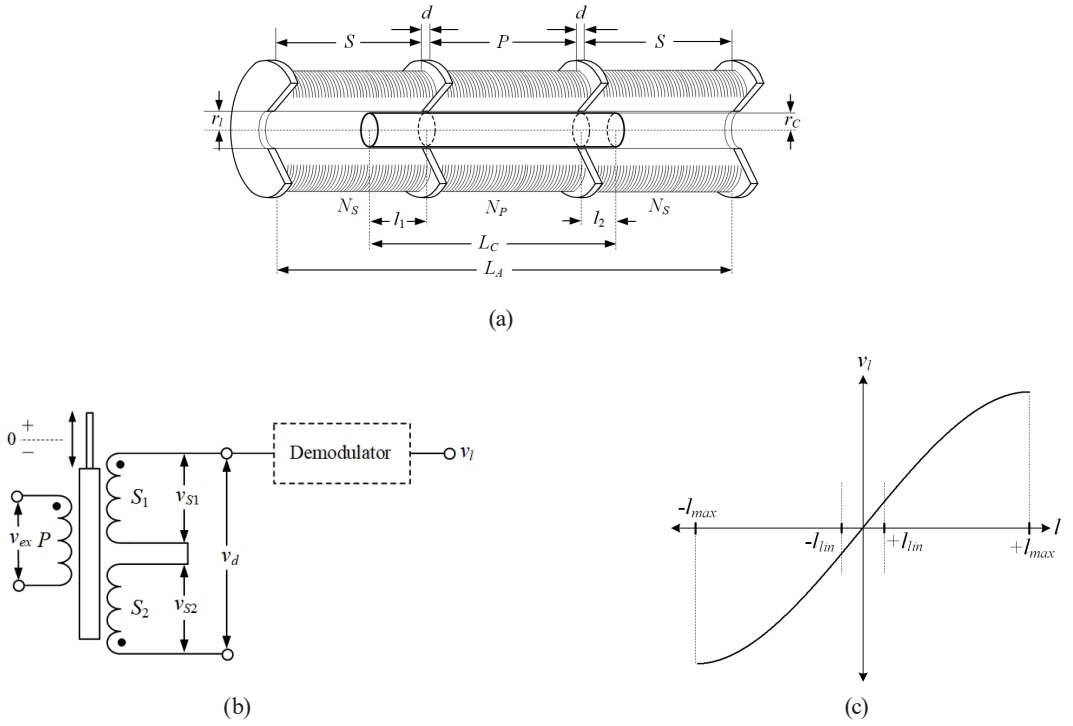

Fig. 1. (a) Structure, (b) schematic diagram, and (c) transfer characteristic of LVDT.

two identical secondary windings are P and S, and their numbers of turns are N_P and N_S, respectively. The gaps between both sides of the primary winding and the two secondary windings are denoted as d. The length and radius of the LVDT core are L_C and r_C, respectively. The excitation signal $v_{ex} = V_P\sin(\omega_{ex}t)$ is applied to the primary winding, where V_P and ω_{ex} denote the peak amplitude and excitation frequency (rad/s) of the excitation signal, respectively. The secondary winding signals v_{S1} and v_{S2} depend on the position of the LVDT core and can be expressed as[3,16,25–27]

$$v_{S1} = \frac{2\pi^2\omega_{ex}v_{ex}N_PN_S\left(2l_2+P\right)}{10^7 L_C Z_P S\ln\left(\frac{r_l}{r_C}\right)}l_1^2 \tag{1}$$

and

$$v_{S2} = \frac{2\pi^2\omega_{ex}v_{ex}N_PN_S\left(2l_1+P\right)}{10^7 L_C Z_P S\ln\left(\frac{r_l}{r_C}\right)}l_2^2, \tag{2}$$

where Z_P denotes the impedance of the primary winding and l_1 and l_2 denote the distances that the moving core penetrates the secondary windings S_1 and S_2, respectively. Owing to the oppositely connected secondary windings, the LVDT signal can be expressed as

$$v_d = v_{S1} - v_{S2} = k_t l\left(1-k_n l^2\right), \tag{3}$$

$$\text{for } k_t = \frac{8\omega_{ex}v_{ex}N_PN_S\left(P+2d+l_0\right)l_0}{10^7 L_C Z_P S\ln\left(\frac{r_l}{r_C}\right)} \text{ and } k_n = \frac{1}{\left(P+2d+l_0\right)l_0}.$$

Here, $l_0 = (l_1 + l_2)/2$ is the position of the LVDT core at the center of the rod and $l = (l_1 - l_2)/2$ is the distance of the LVDT core from l_0. In the structure of the commercial LVDT, the gaps d are much smaller than the length of the primary winding P and the length of the LVDT core $L_C = (3P + 2d)$. Therefore, the LVDT signal v_d can be expressed as

$$v_d = \frac{8\pi^2\omega_{ex}v_{ex}N_PN_S}{10^7 Z_P\ln\left(\frac{r_o}{r_i}\right)}\frac{2P}{3S}\left(l-\frac{l^3}{2P^2}\right) = k_{td}l\left(1-k_{nd}l^2\right), \tag{4}$$

where k_{td} and k_{nd} denote the sensitivity and nonlinear coefficient of the LVDT, respectively. From Eq. (4), the excitation signal v_{ex} is a sinusoidal wave, the peak amplitude of the LVDT signal v_d varies with the position of the LVDT core, and the signal is in the form of an AMSC. Therefore, a synchronous demodulator is required to extract the core position signal v_l from the

LVDT signal v_d, as shown in the dashed rectangle on the right of Fig. 1(b), and v_l can be expressed as

$$v_l = k_{td} l \left(1 - k_{nd} l^2\right). \tag{5}$$

The transfer characteristic of the position signal v_l as a function of the position l of the LVDT core is shown in Fig. 1(c). From Fig. 1(c), the linear operating range l_{lin} of the LVDT for the maximum percentage error ε_{Li} is given by[25–27]

$$l_{lin} = \pm\sqrt{\frac{\varepsilon_{Li}}{k_{nd}}}. \tag{6}$$

Setting a maximum percentage error of $\varepsilon_{Li} = 0.5\%$ and $k_{nd} = 7.75\times10^{-4}$ for the LVDT used in this paper, the linear operating range of the LVDT is calculated from Eq. (6) to be about 2.54 mm. From Eq. (5), if the LVDT core is moved in the linear range l_{lin}, then the core position signal v_l can be approximated as

$$v_l = k_{td} l. \tag{7}$$

From Fig. 1(c), the maximum stroke range l_{pp} of the LVDT can be obtained from the peak-to-peak amplitude of the transfer characteristic as[25–27]

$$l_{pp} = \pm\sqrt{\frac{1}{3k_{nd}}}. \tag{8}$$

The limitation of the maximum stroke range l_{max} of a commercial LVDT depends on the minimum value of the range l_{pp} of the transfer characteristic and the length l_{dem} of the physical dimension of the structure; in other words,[26]

$$l_{max} = \pm\min\left(l_{dem}, l_{pp}\right). \tag{9}$$

The maximum stroke range l_{dem} in terms of the physical dimension of the LVDT is given by[26]

$$l_{dem} = \pm\frac{\left(L_A - L_C\right)}{2}, \tag{10}$$

where L_A denotes the total physical length of the LVDT structure. From Eqs. (8) and (10), the maximum stroke ranges l_{pp} and l_{dem} are ±20.4 and ±6.2 mm, respectively, for the coefficient $k_{nd} = 7.75 \times 10^{-4}$ and the lengths $L_A = 44.1$ mm and $L_C = 31.8$ mm of the LVDT used in this study.

Therefore, the maximum stroke range l_{max} of the LVDT for this study can be determined from Eq. (9) as ±6.2 mm. From Eqs. (4) and (8), the linear operating range of the LVDT can be extended by increasing the number of turns and the length of the primary winding. Unfortunately, increasing the length of the primary winding increases the physical dimension of the LVDT, which is unsuitable for realizing a compact measurement system. If the linear operating range of the LVDT can be extended without changing the LVDT structure, it will be advantageous for many applications.

3. Technique for Extending LVDT Linear Operating Range

The operating range of the LVDT can be extended using its inverse transfer characteristic. A circuit building block to emulate the LVDT transfer characteristic is used in the feedback path of an operational amplifier (opamp) to synthesize the inverse transfer characteristic of the LVDT as shown in Fig. 2.

3.1 Synthesis of LVDT transfer characteristic

The synthesis of the LVDT transfer characteristic in this study is based on the large-signal behavior of an OTA, where the output current *iota* of the OTA in Fig. 3(a) can be expressed as the power series of the hyperbolic tangent:[30, 31]

$$i_{ota} = I_B\left[\frac{v_i}{2V_T} - a_3\left(\frac{v_i}{2V_T}\right)^3 + a_5\left(\frac{v_i}{2V_T}\right)^5 - a_7\left(\frac{v_i}{2V_T}\right)^7 + \cdots\right], \qquad \text{for } v_i \le 2V_T \tag{11}$$

$$a_n = \frac{(-1)^{n-1}\,2^{2n}\left(2^{2n}-1\right)}{2^{2n-1}\pi^{2n}}\left(1+\sum_{j=2}^{\infty}\frac{1}{j^{2n}}\right), \tag{12}$$

where $V_T = kT/q$ is the thermal voltage ($k = 1.38 \times 10^{-23}$ J/K is the Boltzmann constant, $q = 1.602 \times 10^{-19}$ C is the electron charge, and T is the absolute temperature in Kelvin) and I_B is the bias current of the OTA. From Eq. (11), if the current i_{ota} is weighted by a constant w,

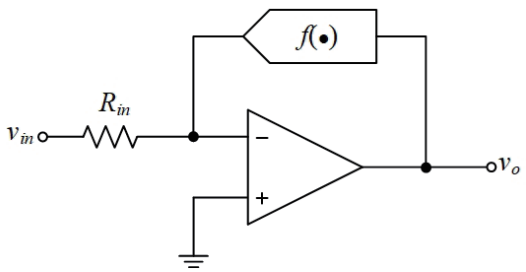

Fig. 2. Synthesis of LVDT transfer characteristic.

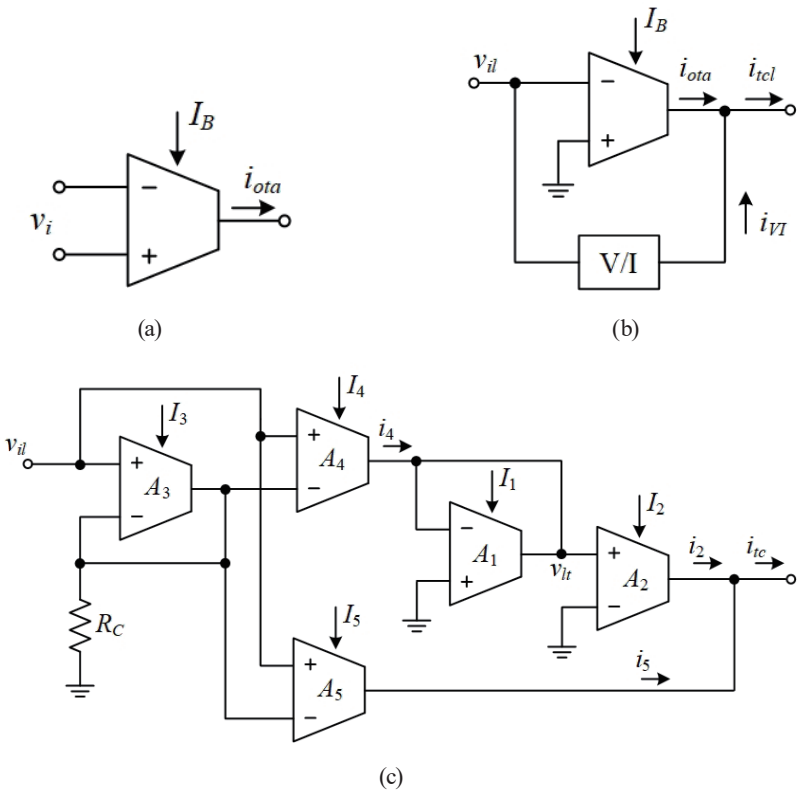

Fig. 3. (a) OTA symbol, (b) principle used to synthesize LVDT transfer characteristic, and (c) circuit used for synthesis of LVDT transfer characteristic.

where $0 < w < 1$, with the condition $a_3 >> a_{2n-1}$ for $n \geq 3$, then Eq. (11) can be approximated as

$$i_{ota} = I_B \left[\frac{w v_i}{2V_T} - \frac{w}{3} \left(\frac{v_i}{2V_T} \right)^3 \right]. \tag{13}$$

The circuit diagram for the synthesis of the LVDT transfer characteristic is shown in Fig. 3(b). From Fig. 3(b), the current i_{tcl} can be expressed as

$$i_{tcl} = \left(2zV_T + wI_B \right) \frac{v_{il}}{2V_T} - \frac{wI_B}{3} \left(\frac{v_{il}}{2V_T} \right)^3, \tag{14}$$

where z denotes the conversion factor of the voltage-to-current converter. If the coefficients of $(2zV_T + wI_B)$ and $wI_B/3$ are set to be equal to the coefficients k_{td} and k_{nd}, respectively, then Eq. (14) can be approximated as the LVDT transfer characteristic. Note that the thermal voltage V_T is dependent on the ambient temperature, which causes inaccuracy in the synthesis of the LVDT transfer characteristic.

To avoid the temperature effect, the temperature-dependent resistance and the voltage-to-current converter formed by the OTAs are provided as shown in Fig. 3(c). From Fig. 3(c), the voltage-to-current converter formed by OTAs A_3 and A_4 converts the voltage signal v_{il} to the current signal i_4. The relationship between v_{il} and i_4 for the bias current $I_4 = I_3$ can be expressed as[31]

$$i_4 = \frac{gm_3}{1 + gm_3 R_C} v_{il}, \tag{15}$$

where gm_3 denotes the transconductance of OTA A_3 and is equal to $I_3/2V_T$. From Eq. (15), if the condition $gm_3R_C >> 1$ is satisfied, then the current signal i_4 can be set as v_{il}/R_C. OTA A_1 acts as a temperature-dependent resistance and converts the current signal i_4 to the voltage signal v_{lt} as follows:

$$v_{lt} = \frac{2V_T}{I_1} i_4 . \tag{16}$$

The voltage signal v_{lt}, which is temperature-dependent, is applied to OTA A_2. It can be clearly seen that the temperature effect in the output current i_2 of OTA A_2 is prevented, and i_2 can be expressed as

$$i_2 = \frac{I_2 v_{il}}{I_1 R_C} - \frac{I_2}{3}\left(\frac{v_{il}}{I_1 R_C}\right)^3 . \tag{17}$$

If the bias current $I_2 = bI_1$ is set, then Eq. (17) can be expressed as

$$i_2 = bI_1\left(\frac{v_{il}}{I_1 R_C}\right) - \frac{bI_1}{3}\left(\frac{v_{il}}{I_1 R_C}\right)^3 . \tag{18}$$

In addition, the inputs of OTA A_5 are connected in parallel with the inputs of OTA A_4. Therefore, the current signal i_5 can be obtained for the condition $gm_{3gm5}R_C >> 1$ as

$$i_5 = \frac{gm_3 I_5}{\left(1 + gm_3 R_C\right) I_3} v_{il} \simeq \frac{I_5 v_{il}}{I_3 R_C} = a\frac{v_{il}}{R_C} . \tag{19}$$

From Eqs. (18) and (19), the current signal i_{tc} can be expressed as

$$i_{tc} = i_5 + i_2 = \left(a + b\right) I_1\left(\frac{v_{il}}{I_1 R_C}\right) - \frac{bI_1}{3}\left(\frac{v_{il}}{I_1 R_C}\right)^3 . \tag{20}$$

It can be clearly seen that Eq. (20) is an odd function in the form of a cubic polynomial. Therefore, the LVDT transfer characteristic can be synthesized using Eq. (20). However, the current signal i_{tc} given by Eq. (20) is valid for $v_{il} \leq I_1 R_C$. Therefore, a scaling factor λ is required for the voltage signal v_{il}. An approximate value of λ can be obtained from the maximum error ε_{max} of the LVDT in its specific linear range l_{lin} as

$$\lambda = \frac{\sqrt{3(\varepsilon_{\max})}}{l_{lin}}. \tag{21}$$

Therefore, Eq. (20) can be rewritten as

$$i_{tc} = \frac{1}{\lambda}\left[(a+b)I_1\left(\frac{\lambda v_{il}}{I_1 R_C}\right) - \frac{bI_1}{3}\left(\frac{\lambda v_{il}}{I_1 R_C}\right)^3\right]. \tag{22}$$

3.2 Proposed technique for extending linear operating range of LVDT

The proposed technique for extending the linear operating range based on the feedback principle of the opamp is shown in Fig. 4. From Fig. 4, the inverting input of opamp OA_1 at node X provides the virtual ground. Therefore, OTA A_5 of Fig. 3(c) can be replaced by the resistance R_f to generate the current i_5 of the circuit in Fig. 3(c). From Eq. (22), the current signal i_{lv} of Fig. 4 for $R_f = R_{C/a}$ is a function of the output voltage v_o, $f(v_o)$, and can be expressed as

$$i_{lv} = f(v_o) = (a+b)\frac{1}{\lambda}\left(\frac{\lambda v_o}{I_1 R_C}\right) - \frac{bI_1}{3\lambda}\left(\frac{\lambda v_o}{I_1 R_C}\right)^3. \tag{23}$$

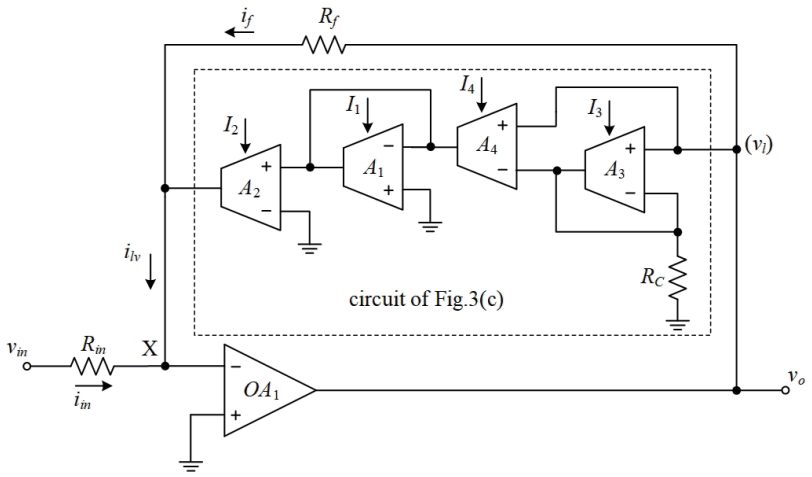

Fig. 4. Proposed circuit.

Practically, the parameters of Eq. (23) of $(a + b)I_1$ and $bI_1/3$ are set to be equal to the coefficients k_{td} and $k_{td}k_{nd}$, respectively, for the synthesis of the LVDT transfer characteristic. From Eq. (21), a and b can be expressed as

$$b = \frac{3k_{td}k_{nd}}{I_1} \tag{24}$$

and

$$a = \frac{k_{td}\left(1 - 3k_{nd}\right)}{I_1}. \tag{25}$$

Equation (23) can be rewritten in the simple form

$$i_{lv} = f(v_o) = \frac{1}{\lambda}\left(\frac{I_1R_C}{R_f} + I_2\right)\frac{\lambda v_o}{I_1R_C} - \frac{I_2}{3\lambda}\frac{\lambda^3 v_o^3}{\left(I_1R_C\right)^3}. \tag{26}$$

From Fig. 4, by writing N as the ratio between the coefficients k_{td} and k_{nd}, $N = k_{td}/k_{nd}$, we can determine the resistance R_f as

$$R_f = \frac{I_1R_C}{\lambda\left(\frac{N}{3} - 1\right)I_2}. \tag{27}$$

The relationship between the current signals i_{lv} and i_{in} of Fig. 4 can be expressed as

$$i_{lv} = -i_{in} \quad \text{or} \quad f(v_o) = -\frac{v_{in}}{R_{in}}. \tag{28}$$

From Eq. (28), the resistance R_{in} is given by

$$R_{in} = \frac{k_{td}\left(1 - k_{nd}l^2\right)I_1R_C}{\lambda\left(\frac{I_1R_C}{\lambda R_f} + I_2\right)}. \tag{29}$$

The output signal v_o can be expressed in the form of the inverse function of the input signal v_{in} as

$$v_o = -f(v_{in}). \tag{30}$$

4. Analysis of Performance

Three major factors adversely affect the performance of the proposed technique. The first factor is the transfer error ε_1 of the current signal i_4 due to the finite transconductance of OTA A_3. The relationship between the current signal i_4 and the voltage v_{il} can be expressed as

$$i_4 = \frac{v_{il}}{R_C}\left[1 - \frac{1}{\left(1 + gm_3 R_C\right)}\right] = \frac{v_{il}}{R_C}\left(1 - \varepsilon_1\right). \tag{31}$$

If gm_3 = 0.019 A/V and R_C = 1 kΩ, then the transfer error ε_1 is about 0.05 or 5%. This error can be minimized by replacing the resistor R_f of Fig. 4 with a variable resistor and fine-tuning the resistance to obtain a converted current i_4 equal to the expected value. The second factor, the variation of the ambient temperature, causes the deviation in the transconductance gm_3 of OTA A_3 due to the change in the thermal voltage V_T and also reduces the accuracy of the current signal i_4. The percentage error ε_2 of the current signal i_4 can be expressed as

$$\varepsilon_2 = \frac{\left|\Delta i_4\right|}{i_4} = \frac{2V_T}{\left(2V_T + I_3 R_C\right)}\frac{\Delta T}{T} \times 100\%, \tag{32}$$

where Δi_4, T, and ΔT denote the change in the current signal i_4, the ambient temperature in Kelvin, and the change in ambient temperature, respectively. If V_T = 25.69 mV at 25°C, ΔT = 10°C, T = 308 K, and I_3 = 1 mA, then the percentage error ε_2 is about 0.08%. The third factor, the residual error ε_3, is caused by the approximation of the LVDT transfer characteristic from the series of the hyperbolic tangent and can be approximated as

$$\varepsilon_3 \simeq \frac{(-1)^{n-1} 2^{2n}\left(2^{2n} - 1\right) b I_1}{2^{2n-1}\pi^{2n} k_{td}}\left(1 + \sum_{j=2}^{\infty}\frac{1}{j^{2n}}\right)\left(\frac{v_{il}}{I_1 R_C}\right)^{n-1} \times 100\% \quad \text{for } n \geq 5. \tag{33}$$

If I_1 = 1 mA, b = 2.33 × 10^{-3}, the peak amplitude v_{il} = 1 V, and R_C = 1 kΩ, then the residual error ε_3 is about 0.03%.

5. Experimental Results

The performance of the proposed technique was confirmed by an experimental implementation. The proposed circuit in Fig. 4 was breadboarded using a commercial device. The LVDT used in this study provides a linear operating range of ±2.5 mm with a percentage error of 0.5% and the coefficients k_{td} and k_{nd} of 94.5 mV/mm/V and 7.75 × 10^{-4} V/Vmm^2, respectively.[25] The operating range l_{pp} was calculated to be ±20.74 mm from k_{nd} using Eq. (8). The physical dimensions of the LVDT were measured as L_A = 44.1 mm and L_C = 31.7 mm. From

Eq. (10), the operating range l_{dem} was determined as ±6.2 mm. Therefore, the maximum operating l_{max} of the LVDT was determined as ±6.2 mm from Eq. (9). The excitation signal $v_{ex} = V_P \sin(\omega_{ext})$ was set, where $V_P = 1$ V and $\omega_{ex} = 15.7$ krad/s or 2.5 kHz. The demodulator in Ref. 16 was used to extract the core displacement signal v_l. An LF351 opamp was used for OA_1 and CA3280 dual OTAs were used for A_1–A_4. The OTA bias currents I_2 and $I_1 = I_3 = I_4$ were set to 100 μA and 1 mA, respectively. The converted resistance R_C was set to 1 kΩ. The resistances R_f and R_{in} were determined from Eqs. (27) and (29) as 81.3 and 6.34 kΩ, respectively. A power supply voltage of $V_{CC} = -V_{EE} = 12$ V was provided. The circuit in the dashed frame of Fig. 4 was used to investigate the performance of the synthesized LVDT transfer characteristic. Figure 5(a) shows the experimental setup of the proposed circuit. The percentage error ε_f for this experiment can be given by

$$\varepsilon_f = \frac{|expected\ value - measured\ value|}{expected\ value} \times 100\% . \tag{34}$$

The measured core displacement signal v_l of the circuit in Fig. 1(b) is shown in Fig. 5(b) for the variation of the LVDT core in the range of ±6.2 mm. The circuit in the dashed frame including the current i_f in Fig. 4 was temporarily separated to investigate the performance of the LVDT transfer characteristic. The maximum error of the transfer characteristic curves in Fig. 5(b) was about 2.93%. Two LVDT signals were used to investigate the circuit performance in this paper. Firstly, the LVDT behavior was emulated using Eq. (5) with an arbitrary function generator, where k_{td} and k_{nd} of 94.5 mV/mm/V and 7.75×10^{-4} V/mm^2, respectively, were set for the LVDT. Firstly, the emulated signal was generated by the arbitrary function generator using an integer value of the core displacement. Therefore, the core displacement of the emulated signal was varied in the range of ±6.0 mm instead of ±6.2 mm to investigate the linearity of the proposed circuit. The emulated signal of ±551.18 mV, corresponding to the movement of the core in the range of ±6.0 mm, was set for the signal v_{in}. Figure 6(a) shows the voltage signal v_o of the inverse

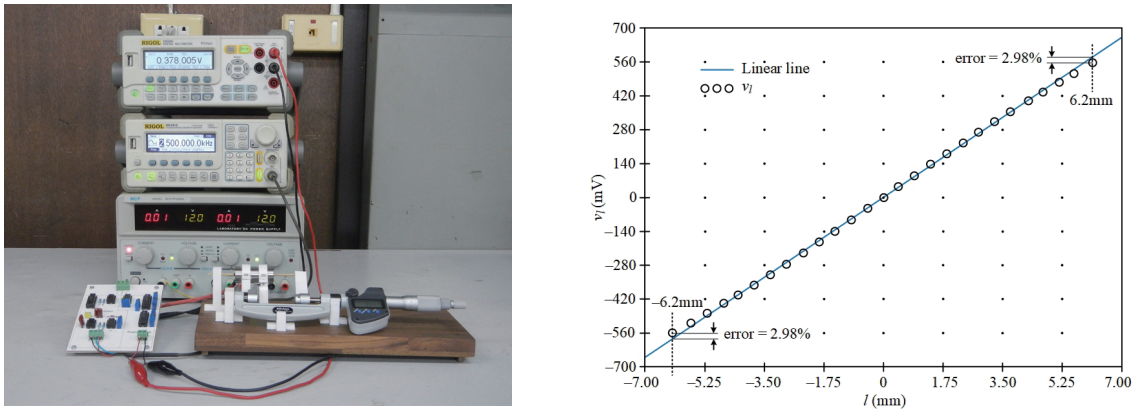

(a) (b)

Fig. 5. (Color Online)(a) Experimental setup and (b) LVDT transfer characteristic.

LVDT transfer characteristic for the emulated signal. It can be seen that the proposed circuit increased the linear operating range of the LVDT.

Secondly, the LVDT signal was applied to the proposed circuit, where the LVDT core was varied in the range of ±6.2 mm or the input signal v_{in} was linearly varied from −568.45 to 568.45 mV. The measured voltage signal v_o for the LVDT signal is shown in Fig. 6(b). The percentage error ε_f of the voltage signal v_o of Fig. 6(b) for the LVDT core that varied in the full stroke range is shown in Fig. 6(c). From Fig. 6(c), the maximum percentage error was about 0.068%. Table 1 shows a comparison of the accuracy, number of components, and cost of the proposed technique with those for the technique recently proposed by Petchmaneelumka *et al.*,[27] which uses the

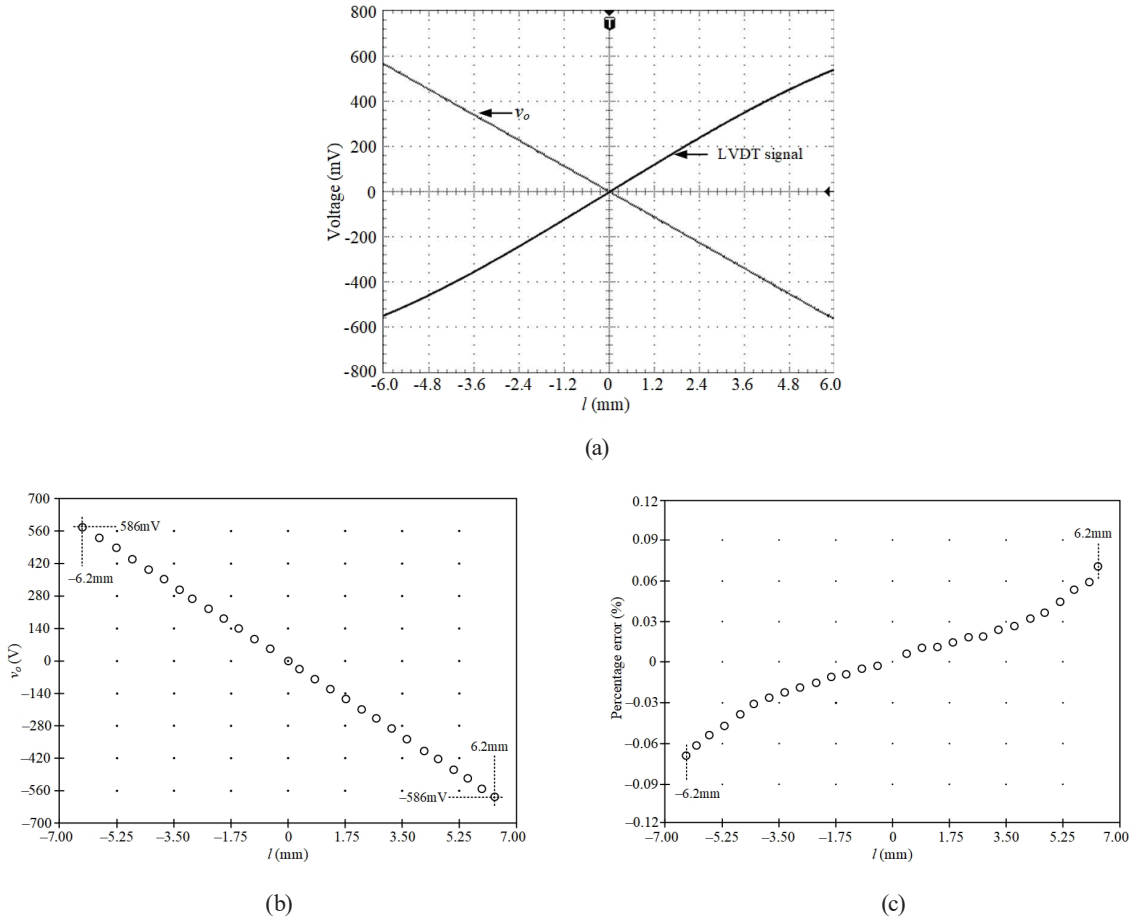

Fig. 6. (a) Measured result for emulated signal, (b) measured result for LVDT signal, and (c) percentage error.

Table 1
Comparison of proposed technique with previous work.[27]

	Accuracy (%) for range of ±6.2 mm	Number of components		Cost (US$)
		Active device	Passive device	
Proposed technique	0.068	2 OTA packages 1 opamp package	3 resistors	12
Previous work[27]	0.35	2 multiplier packages 1 opamp package	2 resistors 2 variable resistors	53

binomial series. Note that the same LVDT was used in this study and Ref. 27. The maximum percentage error of the previous work based on the binomial series was about 0.35% when the LVDT core varied in the range of ±6.2 mm, which is five times that of the proposed technique. It is evident that the proposed technique efficiently extended the linear operating range of the LVDT.

6. Conclusion

We proposed a technique for extending the linear operating range of a commercial LVDT. The large-signal behavior of the OTA was used to synthesize the LVDT transfer characteristic. The synthesized LVDT transfer characteristic was obtained using a synthesized LVDT transfer characteristic circuit connected to the feedback path of an opamp. All devices used in the proposed technique are commercially available. The performance of the proposed technique was analyzed and confirmed by an experimental implementation. The linear operating range of the LVDT used in this study was extended from ±2.54 to ±6.2 mm. The maximum percentage error was about 0.068%. The proposed technique exhibits high accuracy and can be implemented with a simple configuration, small size, and low cost. The proposed technique is suitable for precision measurement systems used in small operating spaces such as miniature robots and scientific and medical equipment.

References

1 R. Pallás-Areny and J. G. Webster: Sensors and Signal Conditioning (John Wiley, New York, 2001).
2 S. C. Saxena and S. B. L. Seksena: IEEE Trans. Instrum. Meas. **38** (1989) 748. https://doi.org/10.1109/19.32186
3 H. K. P. Neubert: Instrument Transducers—An Introduction to Their Performance and Design (Clarendon, Oxford, 1975).
4 J. S. Wilson: Sensor Technology Handbook (Elsevier, Oxford, 2005).
5 G. Chen, B. Zhang, P. Liu, and H. Din: IEEE Sens. J. **15** (2015) 2248. https://doi.org/10.1109/JSEN.2014.2364610
6 Z. Zhang, S. Rau, W. Lee, T. Gammon, and B.C. Johnson: IEEE Trans. Ind Appl. **52** (2016) 5241. https://doi.org/10.1109/TIA.2016.2587775
7 R. W. Kim, C. M. Kim, K. H. Hwang, and S. R. Kim: Appl. Sci. **9** (2019) 1795. https://doi.org/10.3390/app9091795
8 P. Szewczyk and P. Kudyba: Buildings **12** (2022) 172. https://doi.org/10.3390/buildings12020172
9 T. Gu, X. Qian, and P. Lou: Appl. Sci. **11** (2021) 7558. https://doi.org/10.3390/app11167558
10 S. Jang, J. Nam, S. Lee, and J. Oh: Metals **9** (2019) 336. https://doi.org/10.3390/met9030336
11 G. Di Rito, B. Luciano, N. Borgarelli, and M. Nardeschi: Actuators **10** (2021) 230. https://doi.org/10.3390/act10090230
12 L. Blasi, M. Borrelli, E. D'Amato, E. L.E. di Grazia, M. Mattei, and I. Notaro: Aerospace **8** (2021) 39. https://doi.org/10.3390/aerospace8020039
13 M. Mazzoleni, F. Previdi, M. Scandella, and G. Pispola: IEEE Access **7** (2019) 153618. https://doi.org/10.1109/ACCESS.2019.2948781
14 J. G. Webster: Medical Instrumentation Application and Design (Wiley, Hoboken, NJ, USA 2010).
15 F. T. Paziani, B. Di Giacomo, and R. H. Tsunaki: J. Braz. Soc. Mech. Sci. Eng. **29** (2007) 290. https://doi.org/10.1590/S1678-58782007000300009
16 W. Petchmaneelumka, K. Songsuwankit, and V. Riewruja: I.R.E.E. **11** (2016) 340. https://doi.org/10.15866/iree.v11i3.8906
17 R. Casanella, O. Casas, and R. Pallàs-Areny: Meas. Sci. Tech. **16** (2005) 1637. https://doi.org/10.1088/0957-0233/16/8/014
18 C. S. Koukourlis, V. K. Trigonidis, and J. N. Sahalos: IEEE Trans. Instrum. Meas. **42** (1993) 926. https://doi.org/10.1109/19.252529

19 R. González-Landaeta, J. Cota-Ruiz, E. Sifuentes, J. Díaz, and O. Casas: IEEE Trans. Instrum. Meas. **69** (2020) 35. https://doi.org/10.1109/TIM.2019.2895481
20 W. Petchmaneelumka, P. Mano, and V. Riewruja: Sens. Mater. **30** (2018) 2171. https://doi.org/10.18494/SAM.2018.1816
21 J. Tongcharoen, W. Petchmaneelumka, and V. Riewruja: 15th Int. Conf. Control, Automation and Systems (ICCAS, 2015) 1699. https://doi.org/10.1109/ICCAS.2015.7364630
22 P. Veeraian, U. Gandhi, and U. Mangalanathan: AEU – Int. J. Electron. C. **79** (2017) 141. https://doi.org/10.1016/j.aeue.2017.05.037
23 H. Mandal, S. K. Bera, S. Saha, P. K. Sadhu, and S. C. Bera: IEEE Sens. J. **18** (2018) 9501. https://doi.org/10.1109/JSEN.2018.2872510
24 W. Petchmaneelumka, P. Mano, and V. Riewruja: Sens. Mater. **30** (2018) 2171. https://doi.org/10.18494/SAM.2018.1816
25 A. Rerkratn, J. Tongcharoen, W. Petchmaneelumka, and V. Riewruja: Sensors **22** (2022) 3674. https://doi.org/10.3390/s22103674
26 W. Petchmaneelumka, W. Koodtalang, and V. Riewruja: IEEE Sens J. **19** (2019) 5045. https://doi.org/10.1109/JSEN.2019.2902879
27 W. Petchmaneelumka, K. Songsuwankit, J. Tongcharoen, and V. Riewruja: Sens. Mater. **32** (2020) 475. http://doi.org/10.18494/SAM.2020.2407
28 S. K. Mishra, G. Panda, and D. P. Das: IEEE Trans. Instrum. Meas. **59** (2010) 947. https://doi.org/10.1109/TIM.2009.2031385
29 S. Das, D.P. Das, and S.K. Behera: IEEE 8th Conf. Industrial Electronics and Applications (ICIEA, 2013), 1358. http://doi.org/10.1109/ICIEA.2013.6566578
30 A. D. Polyanin and A.V. Manzhirov: Handbook of Mathematics for Engineers and Scientists (Taylor & Francis Group, FL, USA, 2007).
31 V. Riewruja and A. Kaewpoonsuk: Circ. Syst. Signal Process. **25** (2006) 753. https://doi.org/10.1007/s00034-005-1209-1